Volume 48(5): 653–662, 2000
The Journal of Histochemistry & Cytochemistry
http://www.jhc.org

ARTICLE

Seven-color Fluorescence Imaging of Tissue Samples Based on Fourier Spectroscopy and Singular Value Decomposition

Hiromichi Tsurui, Hiroyuki Nishimura, Susumu Hattori, Sachiko Hirose, Ko Okumura, and Toshikazu Shirai

Department of Pathology, Juntendo University School of Medicine (HT,SH,SH,TS); HUSTEC, Toin University Yokohama (HN); CREST, Japan Science and Technology Corporation (HT,KO); and Department of Immunology, Juntendo University School of Medicine (KO), Tokyo, Japan

SUMMARY Seven-color analyses of immunofluorescence-stained tissue samples were accomplished using Fourier spectroscopy-based hyperspectral imaging and singular value decomposition. This system consists of a combination of seven fluorescent dyes, three filtersets, an epifluorescence microscope, a spectral imaging system, a computer for data acquisition, and data analysis software. The spectra of all pixels in a multicolor image were taken simultaneously using a Sagnac type interferometer. The spectra were deconvolved to estimate the contribution of each component dye, and individual dye images were constructed based on the intensities of assigned signals. To obtain mixed spectra, three filter sets, i.e., BI, Gr, and Rd for Alexa488 and Alexa532, for Alexa546, Alexa568, and Alexa594, and for Cy5 and Cy5.5, respectively, were used for simultaneous excitation of two or three dyes. These fluorophores have considerable spectral overlap which precludes their separation by conventional analysis. We resolved their relative contributions to the fluorescent signal by a method involving linear unmixing based on singular value decomposition of the matrices consisting of dye spectra. Analyses of mouse thymic tissues stained with seven different fluorescent dyes provided clear independent images, and any combination of two or three individual dye images could be used for constructing multicolor images.

(J Histochem Cytochem 48:653–662, 2000)

KEY WORDS
fluorescence image
multicolor imaging
hyperspectral imaging
Fourier spectroscopy
singular value decomposition
linear unmixing

Over the past two decades, much of the progress in biology and pathology has resulted from the identification and characterization of new functional molecules within cells. With suspension cells, flow cytometry has provided a means for the simultaneous identification of as many as 10 different proteins within single cells (Roederer et al. 1997; Watanabe et al. 1997; Anderson et al. 1998; Bigos et al. 1999). Flow cytometric information allows the cells within heterogeneous cell populations of cells to be grouped into functional subsets. (Herzenberg et al. 1976).

Correspondence to: Hiromichi Tsurui, Dept. of Pathology, Juntendo University School of Medicine, 2-1-1 Hongo, Bunkyo-Ku, Tokyo 113-8421, Japan. E-mail: tsurui@med.juntendo.ac.jp

Received for publication January 14, 2000; accepted January 19, 2000 (OA5175).

Functional maturation and effector functions of immune cells occur through interactions of different cell populations in particular microenvironments. Therefore, identifications of a variety of functionally distinct cell types and their localization in tissues are essential for estimating events occurring in vivo. At present, filter-based isolation of fluorescence signals is the prevalent system for multicolor analysis of different cell types in tissues. However, if emission spectra of different dyes are overlapping, individual filter-passed signals and standard detectors will yield mixed signals. Therefore, the fluorochromes used in this type of analysis are chosen for their lack of overlap with the other fluorochromes used in the analysis. Because the numbers of dyes with adequately wide and intense non-overlapping emission spectra are limited, the complexity of multicolor analysis of tissues has been restricted.

Recent progress in instrumentation, fluorescent

0022-1554/00/$3.30

dyes, and computer software for numerical analysis has allowed the development of new approaches for multicolor analysis in which the spectrum of a dye mixture can be expressed as a linear combination of the component dye spectra. The signal intensity of each dye can therefore be precisely determined from a single composite spectrum. An interferometric imaging spectrometer (SD-200) (Applied Spectral Imaging; Migdal Haemek, Israel) has recently been introduced in laboratory use (Garini et al. 1996; Malik et al. 1996; Schröck et al. 1996). It has been used mainly for chromosome karyotyping because of its ability to distinguish small differences in spectral signals (Liyanage et al. 1996; Schröck et al. 1997; Veldman et al. 1997; McCormack et al. 1998; MacVille et al. 1999). This apparatus makes it possible to acquire hyperspectral microscope images in a few minutes. A variety of dye combinations and suitable filter sets can be designed to provide efficient excitation of dyes with overlapping excitation spectra and properly distributed emission spectra. Furthermore, to isolate superposed signals, linear unmixing based on singular value decomposition (SVD; Golub and Van Loan 1983; Boardman 1989) can be applied because fluorescence images are well approximated as a linear system.

Combining an efficient imaging spectrometer, appropriate dyes, suitably designed filter sets, and a signal isolation algorithm, we have developed a seven-color fluorescence imaging system for analysis of tissue specimens.

Materials and Methods

Reagents

Succinimidyl ester dyes Alexa488, Alexa532, Alexa546, Alexa568, and Alexa594 and succinimidyl ester dyes Cy5 and Cy5.5 were purchased from Molecular Probes (Eugene, OR) and from Amersham Pharmacia Biotech (Uppsala, Sweden), respectively. Monoclonal antibodies (MAbs) to CD4 (RM4-5), CD8 (53-6.7), CD11c (HL3), CD18 (M18/2), CD44 (IM7), CD45R (RA3-6B2), T-cell receptor β-chain (βTCR, H57-597), and I-A^d/I-E^d (2G9) were purchased from BD PharMingen (Franklin Lakes, NJ). NHS-biotin and streptavidin were from Vector Laboratories (Burlingame, CA), NHS-digoxigenin and goat anti-digoxigenin antibodies from Roche Diagnostics (Mannheim, Germany). For staining of single-cell suspensions, MAb 6B2 was labeled with all the dyes except Cy5.5. Cy5.5 was indirectly stained using biotinylated antibodies and Cy5.5-labeled streptavidin. For tissue staining, MAbs against CD4, CD8, CD11c, I-A^d/I-E^d, and βTCR were labeled with Cy5, Alexa488, Alexa546, Alexa568, and Alexa594, respectively. The MAbs anti-CD18 and anti-CD44 were modified with NHS-digoxigenin and NHS-biotin, respectively. Streptavidin and anti-digoxigenin were labeled with Cy5.5 and Alexa532, respectively. All conjugations were performed in our laboratory according to the manufacturers' instructions.

Filter Design

Three filter sets, designated Bl, Gr, and Rd were designed. Spectral features of the dyes are shown in Table 1, and the construction of the filter sets is shown in Table 2. Bl was used for Alexa488 and Alexa532, Gr was for Alexa546, Alexa568, and Alexa594, and Rd was for Cy5 and Cy5.5. All the filters were purchased from Omega Optical (Brattleboro, VT) and assembled in filter cubes from Olympus (Tokyo, Japan).

Instrumentation

Imaging spectrometer SD-200 was purchased from Applied Spectral Imaging. Details of the structure and the principle for data acquisition have been reported elsewhere (Garini et al. 1996; Malik et al. 1996). The format of the image obtained was of three dimensions, two for spatial (628 × 488) and one for wavelength (70–80 elements). A computer system, originally equipped with 128 MB of memory, a 1.44 MB floppy disk, and 2 GB of HD, was replaced by a newly reconstructed system which consists of a TigerCat system board (Micronics Computers; Fremont, CA), 266 MHz PentiumII (Intel; San Jose, CA), 4 MB graphic board, Xpert@Play (ATI Technologies; Toronto, Ontario, Canada) and 512 MB of memory. As data storage devices, hard disks of 6.4 GB, 10.4 GB, and 15.8 GB (IBM; Armonk, NY), a 640 MB MO driver (Fujitsu; Tokyo, Japan), and CD-R (Plextor; Tokyo, Japan) were used. The epifluorescence microscope BX-60 WI, on which the SD-200 was mounted, was from Olympus. The objective lenses used were Uplan Apo 20×/0.70 and Uplan Apo 40×/0.85.

Signal Isolation

The spectrum of each pixel was expressed as a linear combination of the spectra of component dyes, using the formula shown in Figure 1A. To obtain the abundance vector, the observed spectra were multiplied on the left by a "generalized inverse" of the spectral matrix according to Robbin (1995), using the formula shown in Figure 1B. The numbers of elements in the spectral images ranged from 70 to 80 in our system, and the number of dyes contributing to spectrum of each pixel was two or three. Because the spectral matrices were not square, we used the singular value decomposition (SVD) for the expression of spectral matrices (Press et al. 1986; Boardman 1989; Robbin 1995; Borse 1997). In this way, the rectangular matrix can be decomposed into three matrices: two left and right orthogonal matrices and a singular value normal form (SVNF) matrix located in the middle

Table 1 Spectral features of dyes

Dye	Absorption (nm)	Emission (nm)
Alexa488	495	519
Alexa532	531	554
Alexa546	556	575
Alexa568	578	603
Alexa594	590	617
Cy5	649	670
Cy5.5	675	694

Table 2 Construction of filter sets

Filter set	Exciter	Dichroic mirror	Emitter
Bl	470F35[a]	505DRLP[b]	515EFLP[c]
Gr	546F10	560DRLPO2	565EFLP
Rd	640F20	660DRLP	665EFLP

[a] "F" means full band width at half-maximumal transmission (FWHM).
[b] Dichroic longpass filters transmit a broad range of energy while efficiently reflecting shorter-wavelength energy along another channel in the optical system.
[c] Longpass edge filters reflect more than 99.999% of shorter-wavelength energy that is very close to the transmitted energy.

(Figure 1C). To calculate the generalized inverse of the original matrix, two orthogonal matrices were transposed and reciprocals of principal diagonal components of the middle matrix were taken, followed by reversing their multiplying orders. Abundance vectors were obtained by multiplying observed spectra by the generalized inverse on the left. Calculated abundance vectors for all the pixels construct image planes of component fluorochromes. The software MATLAB (Mathworks; Natick, MA) was used for analyzing detailed spectral characters and for comparing algorithms, and the software ENVI, originally designed for remote sensing (Research Systems; Boulder, CO), was used for actual image analysis.

Sample Preparation

Mice were treated according to the guidelines of Juntendo University Animal facility. Spleen cell suspensions in isotonic PBS, pH 7.4, were prepared from 2-month-old Balb/c mice by gently dispersing cells from tissues using a glass tissue grinder. Cells were stained single-colored, double-colored, and triple-colored with MAb 6B2 conjugated with different fluorochromes. Ten μl of the suspension of stained cell was dropped on a slide glass, sealed with a coverslip, and submitted to analysis. For tissue multicolor immunofluorescence analyses, thymic tissues from 2-month-old New Zealand Black mice were embedded in OCT compound (Miles Scientific; Naperville, IL) and rapidly frozen in liquid nitrogen. Cryostat sections 2 μm thick were fixed in acetone for 10 min and air-dried for 3 min. After immersing in PBS for 5 min, the tissue sections were treated with appropriate concentrations of all antibodies simultaneously, left at room temperature (RT) for 30 min with occasional agitation, washed with PBS, stained with second reagents for 30 min at RT, washed three times with PBS, and sealed with Gel/Mount (Biomeda; Foster City, CA) and a coverslip. The staining reagents contained 0.2% of bovine serum albumin (BSA), 0.05% of Tween-20, and 0.05% of sodium azide. No anti-fade reagent was used.

Data Acquisition and Analysis

Spectral images of blank glass were used as background images. Background images were subtracted from those of all spectral images of samples before analysis. For the construction of spectral libraries, the spectrum of each dye was obtained by averaging signals from the six brightest points in a spectral image of single-stained cells. Linear unmixing based on SVD was performed using these

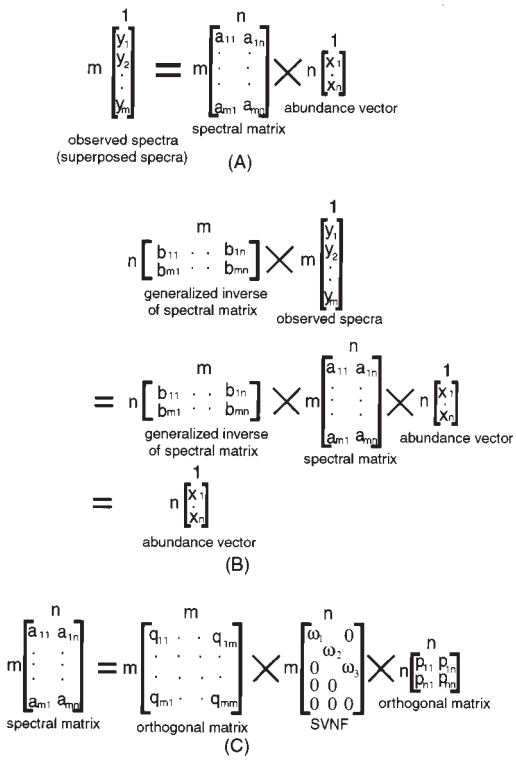

Figure 1 (**A**) The emission spectrum of each dye can be expressed as a column vector, whose dimension, m, is number of elements in the spectra. The spectral matrix consists of the spectra of dyes in same group. The abundance vector is an *n*-dimensional column vector whose values at a certain point are the concentrations of the dyes at a certain point. The observed spectrum of each pixel is a linear combination of dye spectra (superposed spectra), so it is the product of the spectral matrix and abundance vector. (**B**) If the spectral matrix has a "generalized inverse" (Moore–Penrose inverse), the abundance vector is obtained by multiplying the "generalized inverse" on the left. (**C**) SVD decomposes a non-square matrix into three matrices, making it easy to calculate the "generalized inverse" and to estimate the separability of endmembers.

spectral libraries as references. For seven-color imaging, spectral images using Bl, Gr, and Rd filter sets were taken sequentially for one field. After analysis, three of seven decomposed images were used to construct a multicolor image.

Results

In the system we designed, appropriate filter sets are essential. They are required to excite dyes as efficiently as possible, to remove scattered excitation light completely, and to acquire emission spectra as broad as possible. On the basis of spectral features and absorption and emission spectra, shown in Table 1 and Figures 2A–2F, respectively, seven dyes were selected and separated into Bl, Gr, and Rd dye groups. Even though absorption spectra and emission spectra of dyes in each group, particularly in group Bl, were very close (Figures 2A–2F), the exciter, dichroic mirror, and the

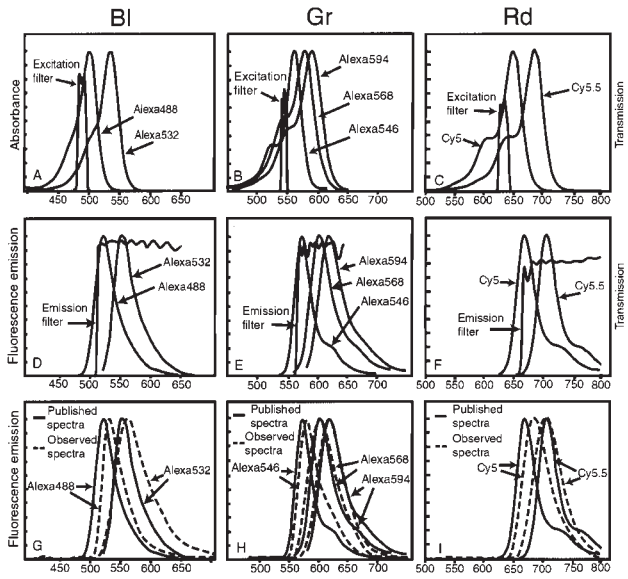

Figure 2 Spectra of dyes and filter sets for each group. Horizontal axes represent wavelength and vertical axes represent absorbance, fluorescence emission, and filter transmission. The wavelength scales are matched within each column. (**A–C**) Absorption spectra of dyes and transmission spectra of excitation filters. (**D–F**) Emission spectra of dyes and transmission spectra of emission filters. (**G–I**) Emission spectra of dyes published (solid lines) and observed (dotted lines). The spectral images of single-color stained cells were taken and corrected by subtracting background images. The spectrum of each dye was obtained by averaging the spectra of the six brightest points in the images. Differences of spectra between the published and the observed are discussed in the text.

emitter filters were required to pass rather broad wavelength regions to realize efficient excitation and light collection. Although the use of these filters caused attenuation of the signal intensity in the short-wavelength portion of each emission region, we could minimize this problem by selection and combination of filters that balance efficient excitation and signal acquisition for each dye group. The spectra of excitation filters used are shown in Figures 2A–2C and those of emission filters are shown in Figures 2D–2F. Exciters, dichroic mirrors, and emitters with steep edges, regions of transmissions closely spaced for simultaneous excitation and acquisition of wide spectra, were selected. (Spectra of dichroic mirrors are not shown.) The spectrum of each dye was obtained by averaging the six brightest points in the image of single-color stained cells (Figures 2G–2I, dotted lines).

As can be seen in Figures 2A, 2B, 2D, and 2E, Alexa532 is efficiently excited with filter set Gr and its longer-wavelength portion of emission passes through this filter-set. Therefore, simultaneous staining of specimens with dyes of both Bl and Gr gave a false-positive estimate for Alexa546. A similar but lesser problem occurred with Alexa594 showing up in the Rd measurements (Figures 2B, 2C, 2E, and 2F). We avoided this problem by adding adequate dummy exposure after image acquisition using Bl and Gr; hence, no false-positive signal from shorter wavelength dye groups affected the following measurements.

Spectra thus obtained were fairly close to those previously published (http://www.probes.com), but there were several differences between the observed and the published spectra. Emission spectra of Alexa488, Alexa546, and Cy5 were apparently shifted to longer wavelengths (to the right) than were found in the published data. This appeared to be mainly due to the blocking of signals in shorter-wavelength regions by the emitter filter (Figures 2D–2I). The spectrum of Cy5.5 appeared to be shifted to shorter wavelengths (to the left). This was due to the decreasing quantum yields of the CCD at long wavelengths. All the spectra observed were wider than those seen in the published data. This can be ascribed to the heterogeneity of dye microenvironments. Because of these three effects, spectra of dyes in the same group were less well separated than expected (Figures 2G–2I). However, they were found to be useful for practical analyses. The spectra thus obtained from images served as spectral libraries for linear unmixing based on SVD.

To confirm the linearity of fluorescence image composition and the validity of SVD for signal isolation, we first examined spectral images of spleen cell suspensions from untreated Balb/c mice 2 months of age, single, double, or triple stained with B-lymphocyte-specific MAb 6B2 (anti-CD45R) conjugated with different dyes in the same group. Spectral images of stained cell suspensions were corrected by subtracting background images of a blank slide glass with coverslip, and were subjected to linear unmixing based on SVD.

Figure 3 shows representative results of single-color stained cells, indicating that each dye signal was clearly isolated. The signal image of a cell stained with a dye was seen only on the "axis" of that dye. This was confirmed by experiments in which aliquots of spleen cell suspension were separately stained with different dyes in the same group (not shown).

Strict signal isolation was also observed with cells either double or triple stained with different dyes in the same group. The images of cells were projected onto "axes" of dye spectra used for staining (Figure 4), thus providing evidence that signals from the same point can be isolated independently and that dyes in a particular location do not affect each other.

On the basis of these findings, we tested the method in seven-color fluorescence imaging of thymic tissue samples obtained from a 2-month-old New Zealand Black mouse. Frozen sections of the thymus were stained simultaneously with seven different reagents, each conjugated with a different dye or hapten. Reagents used were anti-CD8 (Alexa488), anti-CD18 (Alexa532), anti-CD11c (Alexa546), anti-I-A^d/I-E^d (Alexa568),

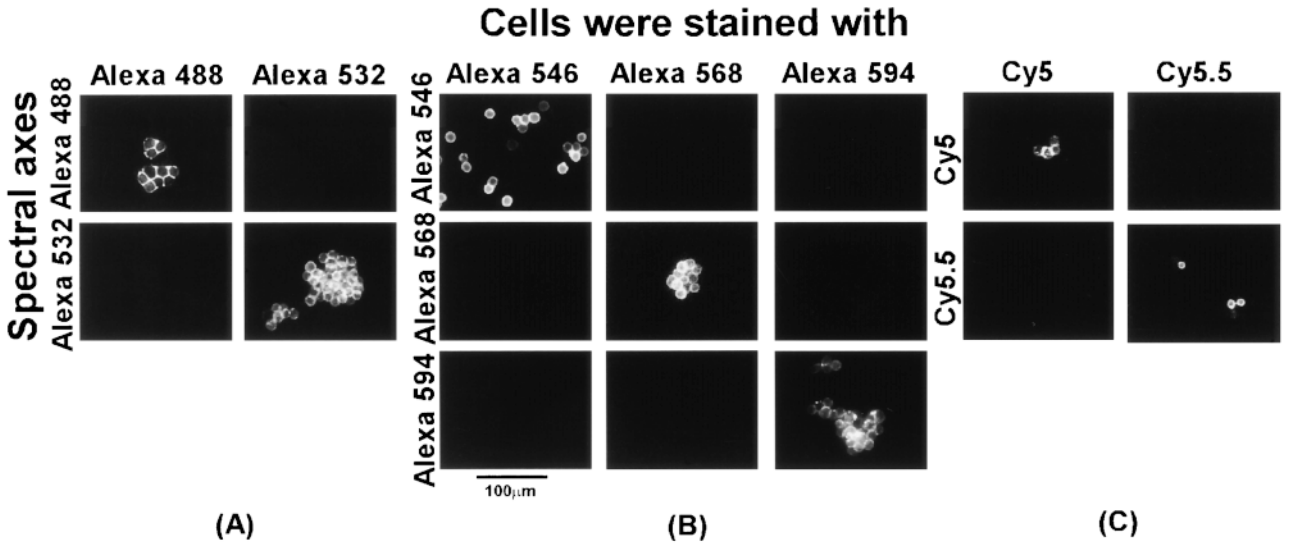

Figure 3 Isolation of spectral signals based on SVD analysis in single-color stained samples. Cells were stained with anti-CD45R (6B2) MAb labeled with each dye directly or indirectly. Spectral images of the cells were taken, background images were subtracted, and the result was subjected to SVD analysis. Images were originally taken using a ×20 objective lens at 628 × 488 pixel resolution and trimmed into 314 × 244 pixels. The name on each column shows the dye used for staining cells. The name shown on the left of each row indicates spectral axis on which spectral images were projected. (**A**) Group Bl; (**B**) Group Gr; (**C**) Group Rd dye. Images can be seen on the "axis" of dyes used for staining but not on the "axes" of other dyes in the same group. The brightness of the images in the same group was adjusted proportional to the originally calculated signal intensities.

anti-βTCR (Alexa594), anti-CD4 (Cy5), and anti-CD44 (Cy5.5).

Precursors of T-cells migrate into the thymus, differentiate, and mature there before moving into the systemic circulation. $CD4^-$ $CD8^-$ cells in early development can be divided into four stages according to the expression of CD25 and CD44; $CD44^+$ $CD25^-$, $CD44^+$ $CD25^+$, $CD44^-$ $CD25^+$, and $CD44^-$ $CD25^-$ (Tanaka et al. 1995). βTCRs are expressed at $CD44^-$ $CD25^+$ stage, and only the cells that succeed in folding a functioning β-chain can proceed to the following developmental stages (β-selection; Mallick et al. 1993). CD44 is also expressed on macrophages. In $CD4^+$ $CD8^+$ cells, TCR α-chains are expressed, and cells expressing complete TCR undergo apoptosis or maturation to $CD4^+$ $CD8^-$ cells and $CD4^-$ $CD8^+$ cells according to the interaction between Class I and Class II molecules expressed on thymic epithelial cells (Tanaka et al. 1995). CD18 (integrin β_2-subunit) combines with CD11a–c-subunits and the αD-subunit, resulting in the formation of LFA-1, Mac-1, p150, 95, and αDβ2, respectively. CD11c is expressed on macrophages, dendritic cells, and NK cells.

Signals of Alexa532 and Cy5.5 were amplified by the digoxigenin–anti-digoxigenin system and the biotin–avidin system, respectively. All other dyes were conjugated directly to the antibodies. After staining, spectral images for Bl, Gr, and Rd group dyes were taken sequentially in the order listed, using corresponding filter sets. In these measurements, dummy exposures were added to remove the false-positive signals from the shorter-wavelength dye groups. Spectral images were analyzed by linear unmixing based on SVD, referring to the spectral libraries previously constructed. We confirmed beforehand that Gel/Mount had no effect on the dye spectra (not shown).

Figure 5 shows that all the signals from these dyes were isolated independently. Medulla, the spreading lower left portion in the image, is surrounded by cortex. βTCRs are expressed more strongly in the medulla than in the cortex, whereas $CD4^+$ cells and $CD8^+$ cells are sparse in the medulla. $I\text{-}A^d/I\text{-}E^d$ is expressed on epithelial cells in both cortex and medulla, in a different distribution pattern. $CD44^+$ cells are distributed mainly in the medulla region. CD18 is mainly expressed on thymocytes both in the cortex and, much more strongly, in the medulla. CD11c is expressed on some populations of $CD18^+$ cells.

Because independent colors included in a color image are limited to three, three different images in Figure 5 were combined to construct multicolor images (Figure 6E). Figures 6A–6C show three-color images of thymus tissue representing different combinations of the seven reagents. In Figure 6A, CD4 (Cy5), CD8 (Alexa488), and βTCR (Alexa594) molecules are assigned blue, red, and green, respectively. The cortex is densely occupied with $CD4^+$ $CD8^+$ cells (either white or violet due to a relatively low expression of βTCR), whereas the medulla shows sparse distribution of the single positive cells (yellow for $CD4^-$ $CD8^+$ and cyan for

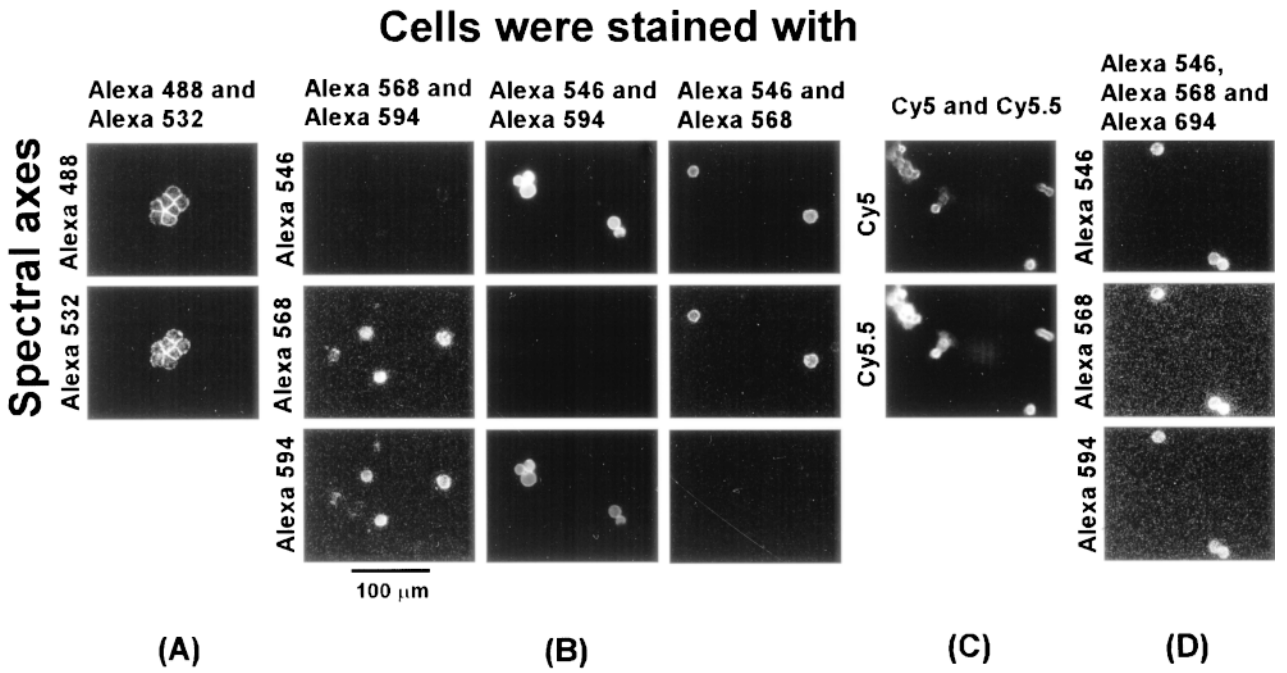

Figure 4 Isolation of spectra based on SVD from double-color stained cells (**A–C**) and triple-color stained cells (**D**). Cells were stained simultaneously with different dyes in the same groups (**A**, Bl; **B**, Gr; **C**, Rd; **D**, Gr). Images were originally taken using a ×20 objective lens at 628 × 488 pixel resolution and combined into 314 × 244 pixels. The name on each column indicates the dye used for staining cells. The name shown on the left of each row indicates the spectral axis on which spectral images were projected. Images can be seen only on the "axes" of dyes spectra used for staining, demonstrating that each superposed signal was isolated independently. The brightness of the images in the same group was adjusted proportional to the calculated signal intensities.

$CD4^+$ $CD8^-$). The distribution of these cells clearly demonstrates the maturation of thymocytes from $CD4^+$ $CD8^+$ cells in the cortex to $CD4^+$ $CD8^-$ or $CD4^-$ $CD8^+$cells in the medulla. In Figure 6B, βTCR (Alexa594), I-A^d/I-E^d (Alexa 568), and CD44 (Cy5.5) are assigned to green, red, and blue, respectively. I-A^d/I-E^d is strongly expressed in the cortex, where expression of βTCR is relatively low. Some $CD44^+$ cells do not overlap βTCR-expressing cells, suggesting them to be macrophages. As shown in Figure 6C, in which CD18 (Alexa532), βTCR (Alexa594), and CD11c (Alexa546) molecules are assigned to red, green, and blue in the image, respectively, the medulla displays preferential accumulation of CD18 high $βTCR^+$ thymocytes (yellow), and the cortex is mainly composed of CD18 low $βTCR^+$ thymocytes. CD11c is expressed on some portions of $CD18^+$ cells (violet).

Discussion

In the present studies, using properly selected dyes, suitably designed filter sets, and a sophisticated mathematical analysis in combination with a recently developed imaging spectrometer, we designed a seven-color fluorescence imaging method for immunostained tissue samples. For dyes, efforts were made to select those with properties of strong signal intensity, low nonspecific binding to tissues, and flexibility of protein modification. We used Alexa488, 532, 546, 568, and 594 for emission at wavelengths from 500 to 650 nm. Among a variety of dyes with emission spectra similar to Alexa series, fluorescein and FluorX (Amersham Pharmacia Biotech) had similar spectral features to Alexa488. However, both showed weaker signals and were less photostable than Alexa488. Addition of *P*-phenylenediamine reduced the photobleaching of fluorescein. However, it considerably broadened the emission spectrum (not shown). Phycoerythrin had an acceptable emission spectrum and a strong signal, but it bleached rapidly. Cy series of dyes Cy2, Cy3, and Cy3.5 (Amersham Pharmacia Biotech) have appropriate emission spectra. However, rates of photobleaching were all far higher than those found in Alexa series dyes (not shown). Texas Red rendered conjugates sticky, causing all the labeled antibodies to agglutinate. In the Alexa series, although Alexa546 was difficult to excite simultaneously with Alexa488, it could be excited efficiently with Alexa594 (Figures 2A and 2B). For dyes to be excited at longer wavelengths, we used Cy5 and Cy5.5. These two dyes showed sufficiently separate spectra, generated fairly strong signals, and gave clear images when measured with a Photometrics PXL1400 camera (not shown). However, because the cooled CCD camera attached to SD-

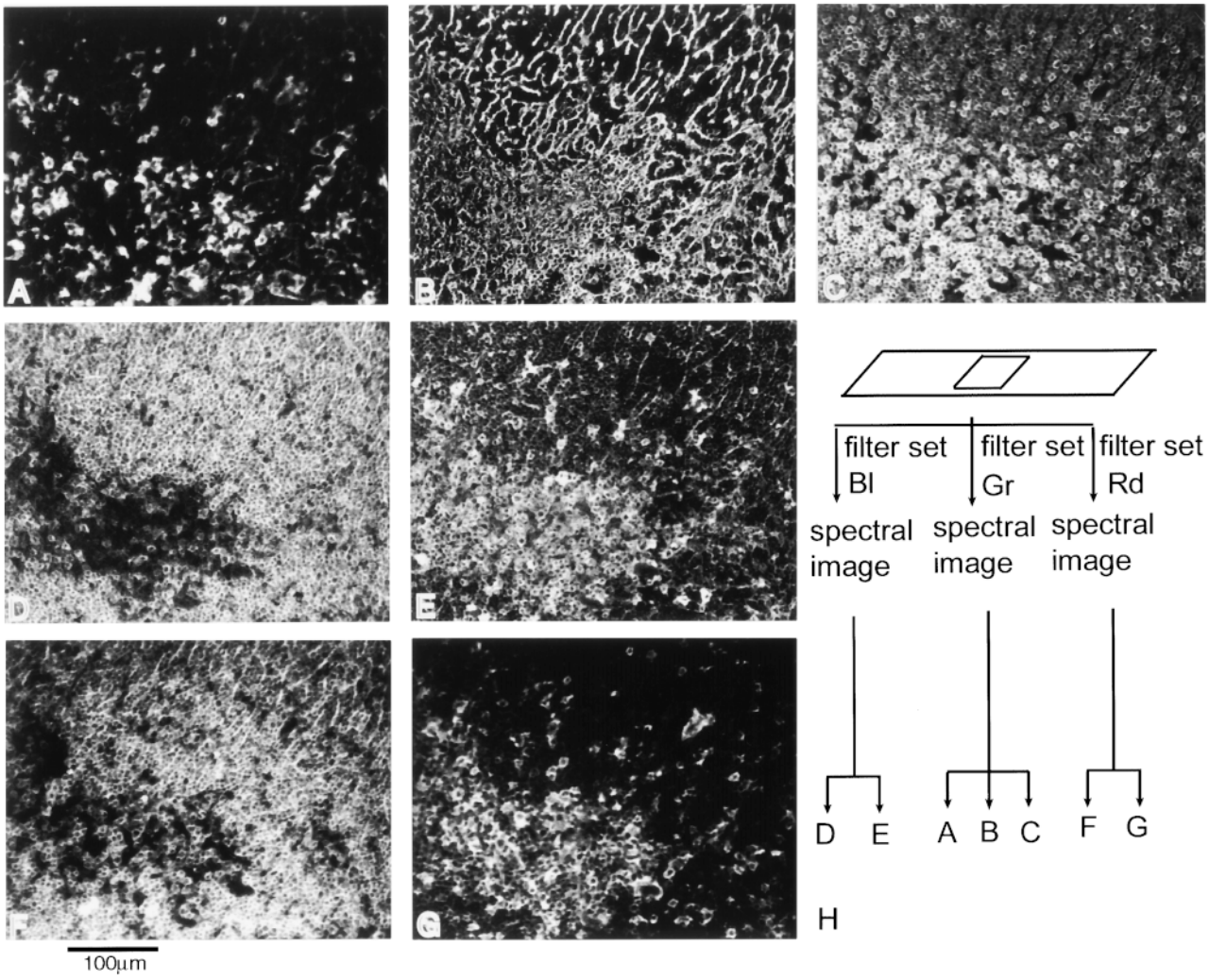

Figure 5 Seven images isolated from three spectral images of a single microscopic field. Frozen sections were prepared from the thymus tissue of a 2-month-old New Zealand Black mouse and stained with seven colors (anti-CD8, Alexa488; anti-CD18, Alexa532; anti-CD11c, Alexa546; anti-I-A^d/I-E^d, Alexa568; anti-βTCR, Alexa594; anti-CD4, Cy5; anti-CD44, Cy5.5). Spectral images were taken using three filter sets, Bl, Gr, and Rd, consecutively. Images were taken using a ×20 objective lens at 628 × 488 pixel resolution. Spectral images were decomposed into images based on the signal intensity of component spectra. Component images of thymus tissue including typical cortex and medulla are shown. **A–C** were obtained from the spectral image using filter set Gr, **D** and **E** using Bl, and **F** and **G** using Rd. **H** illustrates the flow of these processes.

200 had a low sensitivity at long wavelengths, we amplified the signal of Cy5.5 using the biotin-streptavidin system. Cy7 has a spectrum well separated from those of Cy5 and Cy5.5 (maximal absorption is at 743 nm and maximal emission is at 767 nm). However, it was not excited efficiently with the high-pressure mercury lamp, and the sensitivity of the CCD camera at this wavelength was very low.

Many factors were found to affect the shape of observed spectra, i.e. emission filters, the dependence of the CCD camera quantum yield on wavelength, and the microenvironment of the dyes. Because shorter-wavelength regions of the emission spectra of Alexa488, Alexa546, and Cy5 were blocked by the emission filters (Figures 2D–2F), an apparent shift of the emission peaks to longer wavelength occurred. The spectrum of Alexa546 obtained using a filter set with lower pass region is quite similar to the published spectrum (not shown). Most of the observed distortion of these dye spectra can be ascribed to this effect. Indeed, the spectra of Alexa568, Alexa594, and Cy5.5 did not show peak shifts to the longer wavelength. Rather, the spectrum of Cy5.5 was shifted to a shorter wavelength. Because of the decreasing quantum yield of CCD camera with increasing wavelength (from 26% at 650 nm to 14% at 750 nm), the measured spectral peak was shifted to a shorter wavelength. Microenvironments of dyes in tissue samples vary among the dye molecules,

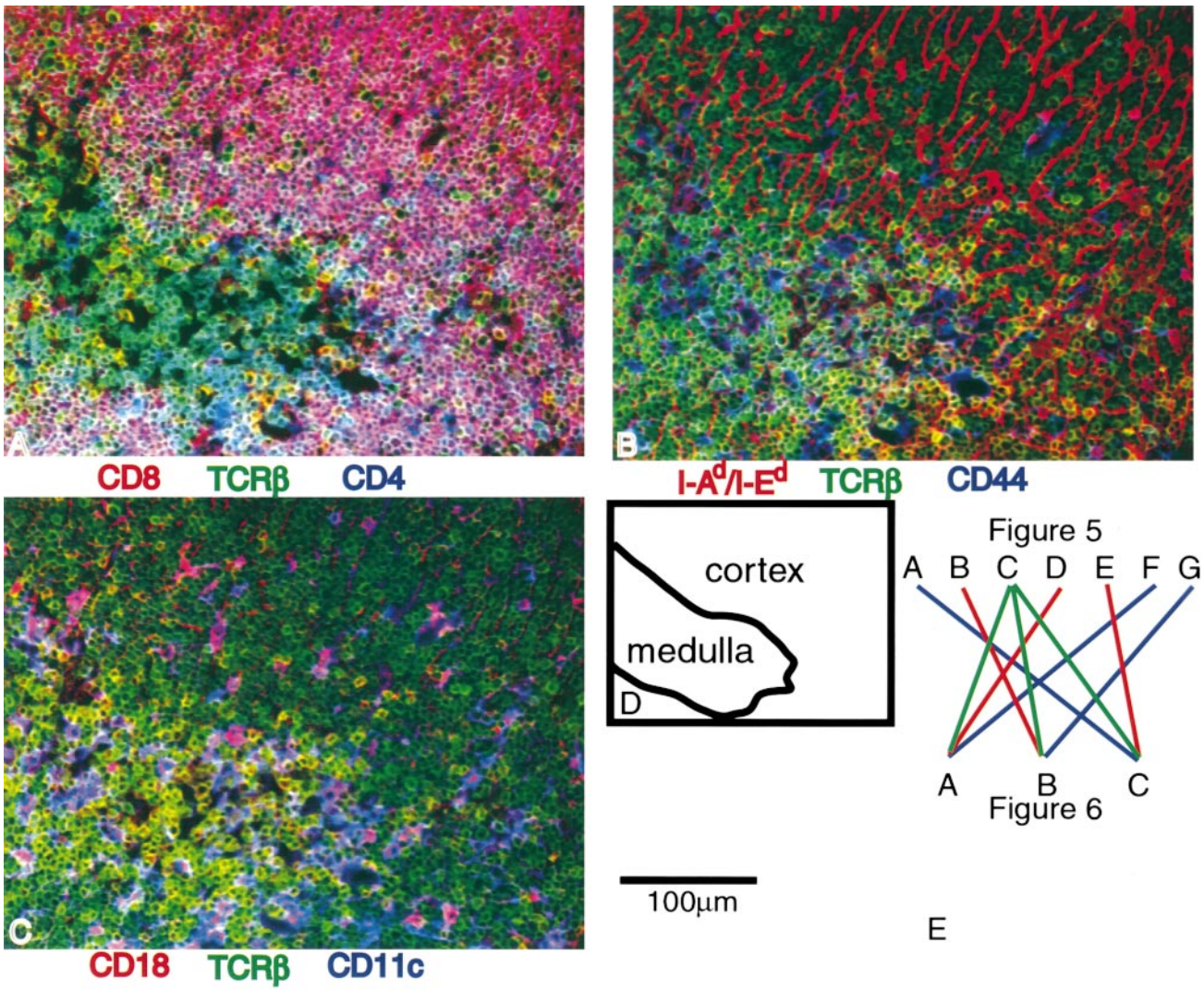

Figure 6 Color images constructed from isolated images. Commonly used color models contain three independent colors, so we combined three isolated images from Figure 5 to form one color image (**E**). (**A**) Anti-CD4, anti-βTCR, and anti-CD8 were assigned to blue, green and red, respectively. (**B**) Anti-I-A^d/I-E^d, anti-βTCR, and anti-CD44 were assigned to red, green and blue, respectively. (**C**), anti-CD11c, anti-βTCR, and anti-CD18 were assigned to blue, green, and red, respectively. A schematic illustration of the structure is shown in **D**. For details, see text.

resulting in subtle difference in emission spectra to broadening of the averaged spectra. We examined images of mixtures of cell suspensions single-color stained with Alexa488 and Alexa532 using very sensitive similarity mapping method. Spectra from cells stained with each dye were divided into four or five classes, and no spectrum was observed in both the regions (not shown). Small variance of spectra from images was observed by another method (Tsurui et al. 1999). This effect may be to some extent responsible for the distortion of spectra of all dyes.

In fluorescence images, the principle of superposition is generally valid. In other words, a fluorescence image behaves like a vector space or, more precisely, a convex body (Schneider 1993), and each spectrum in the image can be represented as a vector. However, the validity of assuming independent superposition may be limited by the presence of non-linear effects such as photobleaching, quenching, fluorescence resonance energy transfer (FRET), and multi-photon excitation. Spectra observed in an actual image result from a mixture of dyes, and, with the assumption of the principle of superposition, they can be expressed as a linear combination of spectra of the component dyes, i.e., the sum of the spectra multiplied by each dye's concentration. Figures 3, 4, and 5 show that the unmixing based on SVD is valid, indicating that a vector space is close approximation to the fluorescence image.

SVD analysis has the advantage that singular values give the volume spanned by the endmembers of the library, defining the extent of the separability of the endmembers. As is shown in Figures 2G–2I, the dye spectra are all well separated. In such cases, the left inverse of matrix A can be calculated as $(A^* A)^{-1}A^*$, where A* represents a conjugate transpose of A. We compared this value with the value obtained by SVD, and the results were consistent within the round-off error of the computations (not shown). This calculation contains only the inverse of square matrix (A* A), and transpose of A.

A karyotyping method based on spectral imaging and combinatorial chromosome staining (spectral karyotyping, SKY) distinguishes 24 human chromosomes, including two sex chromosomes. The principle of this method is to measure spectral angles between the spectrum of the chromosome and those of endmembers of the library and to assign the chromosome's spectrum to the nearest endmember (Garini et al. 1999). Because this method requires that the sources of signals are not superposed on each other, it cannot be applied to general multicolor tissue imaging.

The similarity mapping method measures the distance between the spectra of pixels and classifies them by grouping the nearest ones (Malik et al. 1998). Therefore, this method is also not suitable for analyzing superposed signals. Linear unmixing based on SVD is the method that is best matched to the mathematical structure of fluorescence images.

Photobleaching inevitably occurs during the data collection, making it difficult to obtain high-quality spectra from fluorescence images. To minimize this effect, an instrument with high throughput and efficient signal collection is required. In this regard, monochrometers and bandpass filters are not optimal for fluorescence spectral imaging because only limited portions of emission signals are passed, leading to low quality of acquired spectra and long times for data collection. In this context, the interferometric method works well because of its high throughput and rapid data collection.

As is demonstrated by commonly performed karyotyping, spectral imaging based on the interferometric method provides fairly high resolution at strong magnification. We obtained complete isolation of dye signals used in this study with a ×40 objective lens (not shown). These facts suggest the probability that this method can be applied to cytological investigations.

The multicolor fluorescence imaging method we designed in the present study may be useful for elucidating complex structures consist of several kinds of components or cells that are not distinguishable simultaneously by other means. Furthermore, co-measurement of several factors in an image is available only with this method. Hence, it may be useful for investigating the interactions among several molecules in a cell and, with the help of FACS, for evaluating the role of particular cells in tissue characterized by several markers.

Acknowledgments

We wish to thank to Dr Michael T. Anderson for critical reading of the manuscript and correction of the English. We also thank Sumitomo Electric Industries, Ltd., for the loan of a laboratory room.

Literature Cited

Anderson MT, Baumgarth N, Haugland RP, Gerstein RM, Tjioe T, Herzenberg LA, Herzenberg LA (1998) Pairs of violet-light-excited fluorochromes for flow cytometric analysis. Cytometry 33:435–444

Bigos M, Baumgarth N, Jager GC, Herman OC, Nozaki T, Stovel RT, Parks DR, Herzenberg LA (1999) Nine color eleven parameter immunophenotyping using three laser cytometry. Cytometry 36:36–45

Boardman JW (1989) Inversion of imaging spectrometry data using singular value decomposition. Proc IGARSS'89 Sensing 4:2069–2072

Borse, GJ (1997) Numerical Methods With MATLAB®: A Resource for Scientists and Engineers. Boston, PWS Publishing Company.

Garini Y, Gil A, Bar-Am I, Cabib D, Katzir N (1999) Signal to noise analysis of multiple color fluorescence imaging microscopy. Cytometry 35:214–226

Garini Y, Katzir N, Cabib D, Buckwald RA, Soenksen DG, Malik Z (1996) Spectral Bio-imaging. In Wang XF, Herman B, eds. Fluorescence Imaging Spectroscopy and Microscopy. New York, Wiley, 87–124

Golub GH, Van Loan CF (1983) Matrix Computations. Baltimore, Johns Hopkins University Press

Herzenberg LA, Sweet RG, Herzenberg LA (1976) Fluorescence activated cell sorting. Sci Am 234:108–117

Liyanage M, Coleman A, duManoir S, Veldman T, McCormack S, Dickson RB, Barlow C, Wynshaw–Boris A, Janz S, Wienberg J, Ferguson–Smith MA, Schröck E, Ried T (1996) Multicolor spectral karyotyping of mouse chromosomes. Nature Genet 14:312–315

MacVille M, Schröck E, Padilla–Nash H, Keck C, Ghadimi BM, Zimonjic D, Popescu N, Ried T (1999) Comprehensive and definitive molecular cytogenetic characterization of HeLa cells by spectral karyotyping. Cancer Res 59:141–150

Malik Z, Cabib D, Buckwald RA, Talmi A, Garini Y, Lipson SG (1996) Fourier transform multipixel spectroscopy for quantitative cytology. J Microsc 182:133–140

Malik Z, Rothmann C, Cycowitz T, Cycowitz ZJ, Cohen AM (1998) Spectral morphometric characterization of B-CLL cells verses normal small lymphocytes. J Histochem Cytochem 46: 1113–1118

Mallick CA, Dudley EC, Viney JL, Owen MJ, Hayday AC (1993) Rearrangement and diversity of T cell receptor β chain genes in thymocytes: a critical role for the β chain in development. Cell 73:513–519

McCormack SJ, Weaver Z, Deming S, Natarajan G, Torri J, Johnson MD, Liyanage M, Ried T (1998) Myc/p53 interactions in transgenic mouse mammary development, tumorigenesis and chromosomal instability. Oncogene 16:2755–2766

Press WH, Flannery BP, Teukolsky SA, Vetterling WT (1986) Numerical Recipes. New York, Cambridge University Press

Robbin JW (1995) Matrix Algebra using MINImal MATlab. Wellesley, MA, AK Peters

Roederer M, DeRosa S, Gerstein R, Anderson M, Bigos M, Stovel R, Nozaki T, Parks D, Herzenberg LA, Herzenberg LA (1997) 8 color, 10-parameter flow cytometry to elucidate complex leukocyte heterogeneity. Cytometry 29:328–339

Schneider R (1993) Convex Bodies: The Brunn–Minkowski Theory. New York, Cambridge University Press

Schröck E, du Manoir S, Veldman T, Schoell B, Wienberg J, Ferguson–Smith MA, Ning Y, Ledbetter DH, Bar-Am I, Soenksen D, Garini Y, Ried T (1996) Multicolor spectral karyotyping of human chromosomes. Science 273:494–497

Schröck E, Veldman T, Padilla–Nash H, Ning Y, Spurbeck J, Jalal S, Shaffer LG, Papenhausen P, Kozma C, Phelan MC, Kjeldsen E, Schonberg SA, O'Brien P, Biesecker L, du Manoir S, Ried T (1997) Spectral karyotyping refines cytogenetic diagnostics of constitutional chromosomal abnormalities. Hum Genet 101: 255–262

Tanaka Y, Ardouin L, Gillet A, Lin SY, Magnan A, Malissen B, Malissen M (1995) Early T-cell development in CD3-deficient mice. Immunol Rev 148:171–199

Tsurui H, Lerner JM, Takahashi K, Hirose S, Mitsui K, Okumura K, Shirai T (1999) Hyperspectral imaging of pathology samples. Proc SPIE 3605:273–281

Veldman T, Vignon C, Schröck E, Rowley JD, Ried T (1997) Hidden chromosome abnormalities in haematological malignancies detected by multicolor spectral karyotyping. Nature Genet 15: 406–410

Watanabe N, DeRosa SC, Cmelak A, Hoppe R, Herzenberg LA, Herzenberg LA, Roederer M (1997) Long-term depletion of naive T cells in patients treated for Hodgkin's disease. Blood 90:3662–3672